Eur. Phys. J. A **25**, 29–39 (2005)
DOI 10.1140/epja/i2004-10235-1

THE EUROPEAN PHYSICAL JOURNAL A

Relativistic mean-field study for Zn isotopes

W.Z. Jiang[1,3,a], Z.Z. Ren[2], T.T. Wang[1], Y.L. Zhao[1], and Z.Y. Zhu[1,3]

[1] Institute of Applied Physics, Chinese Academy of Sciences, Shanghai 201800, PRC
[2] Department of Physics, Nanjing University, Nanjing 210093, PRC
[3] Center of Theoretical Nuclear Physics, National Laboratory of Heavy Ion Accelerator, Lanzhou 730000, PRC

Received: 17 November 2004 / Revised version: 11 April 2005 /
Published online: 6 June 2005 –
Communicated by A. Molinari

Abstract. The ground-state properties of Zn isotopes have been investigated using the deformed relativistic mean-field (RMF) theory with the NL-SH and TM1 forces. The π-meson and the spatial component of the ω-meson are taken into account. Shell effects in nuclear sizes and neutron skins are well described. Strong deformations are found for most of Zn isotopes. The shape coexistence of prolate-oblate types exists for a high portion of Zn isotopes. The occurrence of the superdeformed minimum in even isotopes is discussed. The π-meson contribution in ground-state properties of odd Zn isotopes is very limited, whereas the spatial component of the ω-meson that couples to the nonzero vector current in deformed odd nuclei gives rise to the degeneracy breaking of the level with opposite spin projections, playing the role of anti-pairing. The anti-pairing role in odd nuclei and pairing correlations with the Bardeen-Cooper-Schrieffer description in even nuclei are important to give the odd-even difference in charge radii, the prediction of the proton drip line, and possible abundance of the halo structure for neutron-rich isotopes.

PACS. 21.10.Dr Binding energies and masses – 21.60.-n Nuclear-structure models and methods – 27.50.+e $59 \leq A \leq 89$

1 Introduction

Radioactive beams are being used increasingly to produce nuclei far from stability. The experimental data for isotopes of both sides of β-stability are accessible for light nuclei ($Z < 10$) at present, and facilities will be improved for the access to the heavier nuclei in the future. Exotic nuclear structures may emerge possibly at excitation energies and high isospins. These exotic structures such as the nucleon halos or skins can bring about important effects in cross-sections of nuclear reactions and nucleosynthesis. The understanding of the properties of these nuclei is helpful for both nucleosynthesis in astrophysical processes and synthesis of heavy elements. In order to understand exotic nuclear structures at some extreme conditions, it is theoretically of prime importance to investigate isospin-dependent ground-state properties of isotopic chains.

There are quite a few successful descriptions for isotopes at and beyond the valley of stability such as the mass model, nonrelativistic mean-field approach with the various Skyrme-type forces, and relativistic mean-field (RMF) theory. The RMF theory [1–14] seems more powerful since it can dynamically give rise to the spin-orbit interaction associated with shell effects. In the RMF theory the saturation of the nuclear interaction is obtained by a balance between a large attractive potential provided by the scalar σ-meson and a large repulsive potential by the vector ω-meson. The density dependence of the nuclear interaction is appropriately complemented by the nonlinear self-interaction term of σ and ω mesons. The asymmetric energy and isospin dependence in RMF are described through the inclusion of the ρ-meson. The nuclear interaction in RMF is reproduced by the one-meson–exchange summations of various mesons between nucleons.

The RMF models are able to describe the ground-state properties of the isotopic chain from the neutron drip line to proton drip line quite well. In the past, Sharma *et al.* studied the Pb isotopes [15]. The ground-state properties of Kr, Sr, Zr isotopes [16], and quite a few light isotopes in the region $Z = 10$–22 [17] were studied in detail by Lalazissis *et al.* For isotopes of the rare-earth region, Lalazissis *et al.* [18] studied nuclear isotopic shifts and deformation properties systematically. The RMF theory was also applied to the study of the carbon isotopic chain which is abundant for exotic structures by Ren *et al.* [19] and Sharma *et al.* [20]. Most recently, Li *et al.* [21] have investigated the ground-state and pairing properties of Pr isotopic chain in RMF. In the near past, the superdeformed (SD) bands were discovered in the mass region

[a] e-mail: jiangwz@sinap.ac.cn

$A \sim 60$ (Zn isotopes) (see [22–25] and reference therein) which is one of the lightest mass regions where the superdeformation has been observed at high-spin states. SD properties in Zn isotopic chain are shown to be isospin sensitive [26,27]. It is significant to investigate the ground-state properties of Zn isotopes first of all. We will investigate ground-state properties of Zn isotopic chain in RMF. As the superdeformation in odd Zn isotopes was investigated in ref. [28], we will discuss simply the occurrence of superdeformations in some even Zn isotopes.

In general, the RMF framework does not include the spatial component of the ω-meson and the π-meson, since they vanish in spin-saturated nuclei. However, in odd nuclei where the spin of the valence nucleon is not paired, the expectation value of the π-meson does not vanish [29–31], and in deformed odd nuclei the spatial component of the ω-meson turns out to be nonzero [29–33]. We will take into account the π-meson and the spatial component of the ω-meson in deformed RMF [10]. As usual, the π-meson exchange is directly introduced as an effective interaction. In the effective Lagrangian, the pseudo-vector (PV) coupling of the π-meson is preferred, since the pseudo-scalar coupling gives rise to the abnormally large self-energies of nucleons and s-wave scattering length of π-meson-nucleon scattering [14].

We will analyze the ground-state properties of Zn isotopic chain such as binding energies, charge and matter root-mean-square (r.m.s.) radii, and deformations for even and odd nuclei. The role of pairing correlations with the Bardeen-Cooper-Schrieffer (BCS) treatment will be also investigated. In sect. 2, we give the RMF formalism briefly. Numerical results and discussions are presented in sect. 3, and the occurrence of SD minima will be simply touched. The summaries are given in sect. 4. In the appendix, the source terms of the π-meson and the spatial component of the vector meson are given in the axially deformed framework.

2 Formalism

A brief RMF description for finite nuclei is given in this section. The effective Lagrangian is given as

$$\begin{aligned}\mathcal{L} = \overline{\psi}\Big[&i\gamma_\mu\partial^\mu - M_N + g_\sigma\sigma - g_\omega\gamma_\mu\omega^\mu - g_\rho\gamma_\mu\tau_3 b_0^\mu \\ &-\frac{f_\pi}{m_\pi}\gamma^5\gamma^\mu\boldsymbol{\tau}\cdot\partial_\mu\boldsymbol{\pi} - e\frac{1}{2}(1+\tau_3)\gamma_\mu A^\mu\Big]\psi \\ &+U(\sigma)+U(\omega)+\frac{1}{2}(\partial_\mu\boldsymbol{\pi}\partial^\mu\boldsymbol{\pi} - m_\pi^2\pi^2) \\ &+\frac{1}{2}(\partial_\mu\sigma\partial^\mu\sigma - m_\sigma^2\sigma^2) - \frac{1}{4}F_{\mu\nu}F^{\mu\nu} + \frac{1}{2}m_\omega^2\omega_\mu\omega^\mu \\ &-\frac{1}{4}B_{\mu\nu}B^{\mu\nu} + \frac{1}{2}m_\rho^2 b_{0\mu}b_0^\mu - \frac{1}{4}A_{\mu\nu}A^{\mu\nu}\,, \end{aligned} \tag{1}$$

where $\psi, \sigma, \omega, b_0$ and π are the fields of the nucleon, scalar, vector, neutral isovector-vector, and pseudo-scalar mesons, with their masses $M_N, m_\sigma, m_\omega, m_\rho$, and m_π, respectively. A_μ and $A_{\mu\nu}$ are, respectively, the field of the photon and its field strength tensor. g_i $(i = \sigma, \omega, \rho)$ and f_π are the corresponding meson-nucleon couplings. τ and τ_3 are the isospin Pauli matrix and its third component. $F_{\mu\nu}$, $B_{\mu\nu}$ and $A_{\mu\nu}$ are the strength tensors of ω, ρ mesons, and photon, respectively:

$$\begin{aligned} &F_{\mu\nu} = \partial_\mu\omega_\nu - \partial_\nu\omega_\mu\,, \qquad B_{\mu\nu} = \partial_\mu b_{0\nu} - \partial_\nu b_{0\mu}\,, \\ &A_{\mu\nu} = \partial_\mu A_\nu - \partial_\nu A_\mu\,. \end{aligned} \tag{2}$$

The self-interacting potential of σ and ω mesons read, respectively,

$$U(\sigma) = \frac{1}{3}g_2\sigma^3 + \frac{1}{4}g_3\sigma^4, \qquad U(\omega) = \frac{1}{4}c_3(\omega_\mu\omega^\mu)^2\,, \tag{3}$$

In RMF, only the third components of isovector mesons ρ and π, *i.e.* b_0 and π_0, survive due to the charge conservation. Though the PV coupling of the π-meson is not renormalizable, we remind ourselves here that we work on the effective interactions. The pseudo-vector coupling f_π is taken as the experimental value 0.9708.

Using the Euler-Lagrangian equation, the Dirac equation of motion is given as

$$\begin{aligned}\Big(&i\gamma_\mu\partial^\mu - M_N + g_\sigma\sigma - g_\omega\gamma_\mu\omega^\mu - g_\rho\gamma_\mu\tau_3 b_0^\mu \\ &-\frac{f_\pi}{m_\pi}\gamma^5\gamma^\mu\tau_3\cdot\partial_\mu\pi_0 - e\frac{1}{2}(1+\tau_3)\gamma_\mu A^\mu\Big)\psi_i = 0\,. \end{aligned} \tag{4}$$

The mesons and photon obey the following equations:

$$(\partial^2 + m_\sigma^2)\sigma = g_\sigma\sum_i^A\bar{\psi}_i\psi_i - g_2\sigma^2 - g_3\sigma^3\,, \tag{5}$$

$$\partial^\mu F_{\mu\nu} + m_\omega^2\omega_\nu = g_\omega\sum_i^A\bar{\psi}_i\gamma_\nu\psi_i - c_3\omega_\nu\omega_\mu^2\,, \tag{6}$$

$$\partial^\mu B_{\mu\nu} + m_\rho^2 b_{0\nu} = g_\rho\sum_i^A\bar{\psi}_i\tau_3\gamma_\nu\psi_i\,, \tag{7}$$

$$(\partial^2 + m_\pi^2)\pi_0 = \frac{f_\pi}{m_\pi}\sum_i^A\partial_\mu(\bar{\psi}_i\gamma^5\gamma^\mu\tau_3\psi_i)\,, \tag{8}$$

$$\partial^\mu A_{\mu\nu} = e\sum_i^A\bar{\psi}_i\frac{1+\tau_3}{2}\gamma_\nu\psi_i\,, \tag{9}$$

where A is the nucleon number of the system.

In the RMF approximation, the Dirac equation can be written explicitly as

$$\begin{aligned}\Big(&-i\boldsymbol{\alpha}\cdot\nabla + \beta M_N^* + g_\omega\omega^0(\mathbf{r}) - g_\omega\boldsymbol{\alpha}\cdot\boldsymbol{\omega}_v(\mathbf{r}) + g_\rho\tau_3 b_0^0(\mathbf{r}) \\ &-g_\rho\tau_3\boldsymbol{\alpha}\cdot\mathbf{b}_0(\mathbf{r}) + \frac{f_\pi}{m_\pi}\gamma^5\tau_3\boldsymbol{\alpha}\cdot\nabla\pi_0(\mathbf{r}) \\ &+e\frac{1}{2}(1+\tau_3)A^0(\mathbf{r})\Big)\psi_i(\mathbf{r}) = 0 \end{aligned} \tag{10}$$

with $M_N^* = M_N - g_\sigma\sigma(\mathbf{r})$. Here the spatial vector of the electro-magnetic field is neglected since it is much smaller than the counterpart of the vector meson in the

strong-interaction system. For mesons and photon, equations are given as

$$(-\Delta + m_\sigma^2)\sigma(\mathbf{r}) = g_\sigma \sum_i^A \bar{\psi}_i(\mathbf{r})\psi_i(\mathbf{r}) - g_2\sigma^2(\mathbf{r}) - g_3\sigma^3(\mathbf{r}) = g_\sigma \rho_s(\mathbf{r}) - g_2\sigma^2(\mathbf{r}) - g_3\sigma^3(\mathbf{r}), \quad (11)$$

$$(-\Delta + m_\omega^2)\omega^0(\mathbf{r}) = g_\omega \sum_i^A \bar{\psi}_i(\mathbf{r})\gamma^0\psi_i(\mathbf{r}) - c_3\omega^0\omega_\mu^2 = g_\omega \rho_B(\mathbf{r}) - c_3\omega^0\omega_\mu^2, \quad (12)$$

$$(-\Delta + m_\rho^2)b_0^0(\mathbf{r}) = g_\rho \sum_i^A \bar{\psi}_i(\mathbf{r})\tau_3\gamma^0\psi_i(\mathbf{r}) = g_\rho \rho_3(\mathbf{r}), \quad (13)$$

$$(-\Delta + m_\pi^2)\pi_0(\mathbf{r}) = \frac{f_\pi}{m_\pi} \sum_i^A \nabla \cdot (\bar{\psi}_i(\mathbf{r})\gamma^5\boldsymbol{\gamma}\tau_3\psi_i(\mathbf{r})) = \frac{f_\pi}{m_\pi}\rho_\pi(\mathbf{r}), \quad (14)$$

$$-\Delta A^0 = e\sum_i^A \bar{\psi}_i(\mathbf{r})\frac{1+\tau_3}{2}\gamma^0\psi_i(\mathbf{r}) = e\rho_p(\mathbf{r}). \quad (15)$$

For the spatial part of vector mesons, there is only the angular part

$$(-\Delta + m_\omega^2)\boldsymbol{\omega}_\varphi(\mathbf{r}) = g_\omega \sum_i^A \bar{\psi}_i(\mathbf{r})\boldsymbol{\gamma}\psi_i(\mathbf{r}) + c_3\omega_\varphi\omega_\mu^2 = g_\omega \mathbf{j}_{\omega_\varphi}(\mathbf{r}) + c_3\omega_\varphi\omega_\mu^2, \quad (16)$$

$$(-\Delta + m_\rho^2)\mathbf{b}_{0\varphi}(\mathbf{r}) = g_\rho \sum_i^A \bar{\psi}_i(\mathbf{r})\tau_3\boldsymbol{\gamma}\psi_i(\mathbf{r}) = g_\rho \mathbf{j}_{b_\varphi}(\mathbf{r}), \quad (17)$$

where ρ_s, ρ_B, ρ_3 and ρ_p are different densities, and $\mathbf{j}$'s are vector currents. In the spherical or spin-saturated deformed nuclei, the spatial parts of vector mesons vanish. Since the spatial component of the ρ-meson is small with comparison to that of the ω-meson, we will neglect it in the actual calculation. To see how the π-meson and the spatial component of the vector meson have nonzero contributions, we will give in the appendix their source terms explicitly in the axially symmetric framework for odd nuclei and show how they vanish for even nuclei.

The total binding energy is defined as

$$E_B = A \times M_N - E, \quad (18)$$

where E is the total system energy:

$$\begin{aligned} E = {} & E_N + E_\sigma + E_{\sigma NL} + E_{\omega_0} + E_{b_0} + E_c \\ & + E_{CM} + E_{\omega_v} + E_{\mathbf{b}_v} + E_\pi = \\ & \sum_\alpha E_\alpha - \frac{1}{2}\int \mathrm{d}^3r(g_\sigma\sigma(\mathbf{r}) + \frac{2}{3}g_2\sigma^3(\mathbf{r}) + \frac{1}{2}g_3\sigma^4(\mathbf{r})) \\ & - \frac{1}{2}g_\omega \int \mathrm{d}^3r\omega_0(\mathbf{r})\rho_B(\mathbf{r}) - \frac{1}{2}g_\rho \int \mathrm{d}^3r b_0(\mathbf{r})\rho_3(\mathbf{r}) \\ & + \frac{1}{2}g_\omega \int \mathrm{d}^3r\boldsymbol{\omega}_\varphi(\mathbf{r})\mathbf{j}_{\omega_\varphi}(\mathbf{r}) + \frac{1}{2}g_\rho \int \mathrm{d}^3r\mathbf{b}_{0\varphi}(\mathbf{r})\mathbf{j}_{b\varphi}(\mathbf{r}) \\ & - \frac{1}{2}e\int \mathrm{d}^3rA_0(r)\rho_c(r) - \frac{3}{4}41A^{1/3} + E_\pi \end{aligned} \quad (19)$$

with α the collection of good quantum numbers, and

$$E_\pi = -\frac{f_\pi}{2m_\pi}\int \mathrm{d}^3\mathbf{r}\pi_0(\mathbf{r})\nabla\cdot(\psi^\dagger(\mathbf{r})\boldsymbol{\Sigma}\tau_3\psi(\mathbf{r})). \quad (20)$$

The pairing correlation will be taken into account for even nuclei in calculations using the BCS theory. The details of the treatment may be found in ref. [10]. We use constant pairing gaps which are obtained using the prescription of Möller and Nix [34]

$$\Delta_n = \frac{4.8}{N^{1/3}}, \qquad \Delta_p = \frac{4.8}{Z^{1/3}} \quad (21)$$

with N and Z the neutron and proton number, respectively. In deformed odd nuclei, there exists a nonzero vector current which results in the breaking of the time-reversal symmetry and the spin $\pm\Omega_i$ degeneracy is therefore broken. Calculations for odd-Z Pr isotopes [21] even without including the vector current show that the pairing correlation has very limited contributions in isotopes within drip lines. Considering these factors, we omit the pairing correlation treatment in odd Zn isotopes.

3 Results and discussions

The RMF equations are solved in the axially deformed framework. In the deformed system, we refer to treatments of [10], namely solve the Dirac equations together with meson equations by the expansion in the harmonic-oscillator basis. The Dirac and meson equations are expanded separately in the harmonic-oscillator basis with the respective oscillator quantum number N_F and N_B. The numerical calculations follow ref. [10] and here we take $N_F = N_B = 12$.

We use the RMF parameter sets NL-SH [12] and TM1 [13] to perform calculations. The parameter set NL-SH is as follows: $M_N = 939.0\,\mathrm{MeV}$, $m_\sigma = 526.059\,\mathrm{MeV}$, $m_\omega = 783.0\,\mathrm{MeV}$, $m_\rho = 763.0\,\mathrm{MeV}$, $g_\sigma = 10.4436$, $g_\omega = 12.9451$, $g_\rho = 4.3828$, $g_2 = -6.9099\,\mathrm{fm}^{-1}$, $g_3 = -15.8337$. TM1 parameters are the following: $M_N = 938.0\,\mathrm{MeV}$, $m_\sigma = 511.198\,\mathrm{MeV}$, $m_\omega = 783.0\,\mathrm{MeV}$, $m_\rho = 770.0\,\mathrm{MeV}$, $g_\sigma = 10.0289$, $g_\omega = 12.6139$, $g_\rho = 4.6139$, $g_2 = 27.2325\,\mathrm{fm}^{-1}$, $g_3 = 0.6183$, and $c_3 = 71.5075$. The NL-SH and TM1 sets are good choices to describe the isotopic chains from the neutron drip line to the proton drip line.

In the following, we will investigate the binding energies, nuclear sizes (radii), isotope shift, quadrupole deformations, shape coexistence, SD minima in even nuclei, and positions of drip line nuclei, together with the role of pairing correlations in BCS for the Zn isotopic chain. The contributions of the π-meson and spatial component of the ω-meson will be also discussed at last.

3.1 Binding energies

Binding energies of Zn isotopic chain in the deformed RMF calculations with NL-SH and TM1 parameter sets

Table 1. The binding energies E_B (in MeV) of Zn isotopes obtained for the lowest-energy state with the forces NL-SH and TM1. The empirical values (Expt.) available are also shown for comparison. The labels I and II stand for the first (prolate) and second (oblate) minima of the ground state, respectively.

	NL-SH		TM1				NL-SH		TM1		
A	I	II	I	II	Expt.	A	I	II	I	II	Expt.
52	380.11	380.06	380.70	380.84		76	652.58	651.02	652.17	650.37	651.99
53	398.09		397.32			77	657.82		656.61		656.63
54	417.28	416.22	417.79	416.08	418.95	78	664.43	663.83	662.64	661.75	663.31
55	434.67		434.37		435.38	79	668.99	667.67	666.15	665.37	668.10
56	452.55	451.62	451.86	450.43	454.25	80	675.82		672.19		674.01
57	467.91		466.27		469.28	81	676.18	675.89	673.05	672.75	676.43
58	485.65		482.93		486.96	82	680.93	680.88	677.74	677.70	680.44
59	497.12		496.70		500.00	83	681.90		679.52		
60	511.32	509.67	510.67	509.14	514.99	84	685.76	684.29	683.75	682.43	
61	522.70		521.69		525.22	85	686.46	684.24	684.70	682.65	
62	534.25	532.79	534.56	533.47	538.12	86	690.06	688.68	688.73	687.75	
63	543.91	542.38	543.92	543.66	547.23	87	690.63	689.54	689.49	688.72	
64	554.74	554.32	555.90	555.99	559.09	88	693.50	693.15	692.71	692.70	
65	562.29	561.87	564.05	563.96	567.07	89	692.58	692.46	692.55	692.30	
66	573.05	573.32	574.99	575.50	578.13	90	696.11	696.57	695.85	696.36	
67	580.18	580.00	582.64	582.71	585.19	91	695.55	695.81	695.09	694.64	
68	590.94	591.36	593.61	593.98	595.38	92	698.62	699.24	698.71	699.35	
69	597.52	598.07	599.85	600.42	601.87	94	700.90	701.85	701.18	702.22	
70	608.10		611.14		611.08	96	703.20	703.93	703.79	704.50	
71	613.66	614.10	616.36	615.79	616.92	98	706.09	706.09	706.97	706.97	
72	623.04		625.19		625.79	100	708.88	708.88	709.87	709.86	
73	629.21	628.59	630.71	629.60	631.15	102	709.02	709.02	709.35	709.35	
74	638.65	637.50	639.25	638.10	639.52	104	708.74	708.20	707.78	707.40	
75	644.53	642.96	645.55		644.35						

are given in table 1. The theoretical values are the lowest energies of ground states. As Zn isotopes are considered to be deformed, the RMF minimization is performed both for a prolate and an oblate shape. The binding energies for the first minimum (I) and the second minimum (II) (if existent) correspond to the prolate and oblate shapes, respectively. Available experimental values from the mass compilation of Audi and Wapstra [35] are also listed for comparison. The binding energies with both the NL-SH and TM1 sets are in good agreement with the experimental values available. The good agreement with experimental data for the odd isotopic binding energies indicates that our treatment for odd isotopes is reasonable.

3.2 Nuclear radii and isotope shift

The nuclear size in quantum many-body systems is an important phenomenological number. For nuclei of β-stability, it is well known that the nuclear size is proportional to $A^{1/3}$. However, in the isotopic chain from the proton drip line to the neutron drip line there exists a so-called isotope shift [15,16,18] which makes the nuclear size deviate from the $A^{1/3}$ relation. The RMF theory was for the first time able to describe the isotope shift [15,18,21]. Though the experimental data about charge r.m.s. radii and isotope shifts are scarce, the prediction of the isotope shift is still helpful to understand the isospin dependence of nuclear sizes and shell effects.

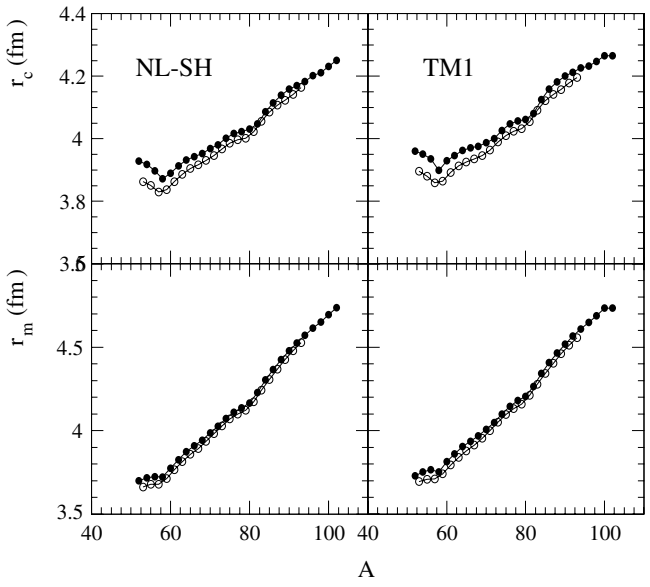

Fig. 1. The charge and matter r.m.s. radii of Zn isotopes: r_c and r_m. The empty circle is for odd isotopes and the solid one is for even isotopes. The left panel is calculated with the NL-SH and the right one is with the TM1.

Charge and matter radii of Zn isotopes are shown in fig. 1. The NL-SH and TM1 forces reproduce similar results. There is a minimum in the isotope shift curves. For

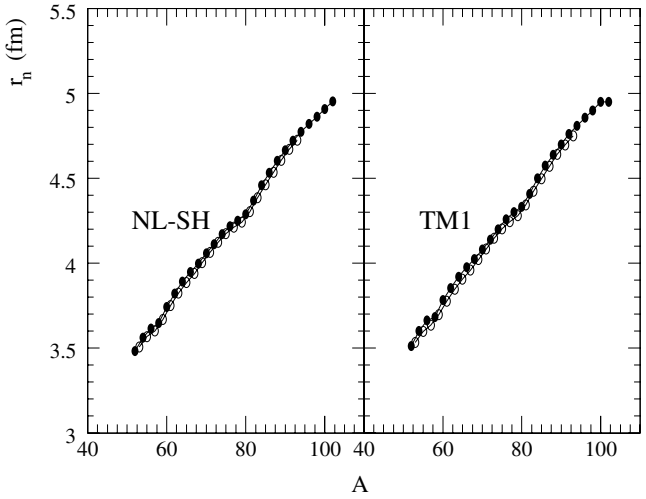

Fig. 2. The same as shown in fig. 1 but for the neutron r.m.s. radii.

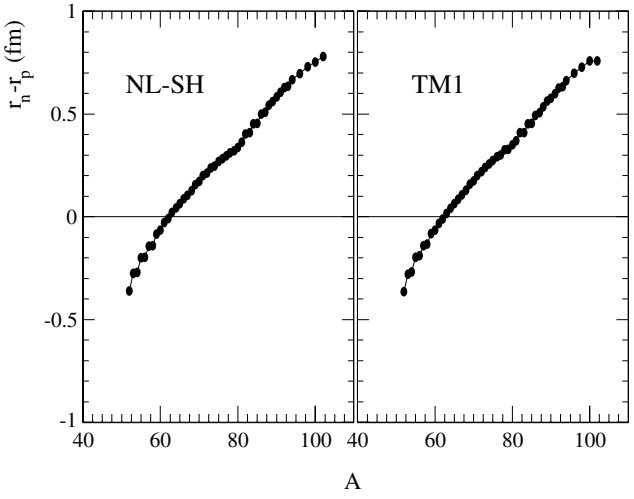

Fig. 3. The neutron skin thickness $(r_n - r_p)$ of Zn isotopes from the proton-rich side to the neutron-rich side.

neutron-deficient nuclei, the isotope radius rises abnormally with the decrease of neutron number, which also exists for many other isotopic chains. Two kinks are found at the neutron magic number $N = 28$ and 50, as shown clearly in fig. 1. The appearance of the kink may be related to the nuclear deformation and shell effect. The deformation contributes partly to the increase of the nuclear size [15,18]. The semi-magic nuclei have a strong shell effect and a smaller deformation than the neighboring nuclei, leading to the existence of the kink. In the nonrelativistic approach of Skyrme, it is difficult to explain the kink unless the isospin-dependent spin-orbit interaction is carefully modified [36]. The success of the description for the isotope shift and kink in the RMF theory is attributed to the isospin-dependent spin-orbit potential determined dynamically by the Dirac structure of spinors.

Different from the charge and matter radii, the neutron r.m.s. radii, as shown in fig. 2, increase monotonously with the rise of neutron number. Compared to the neutron radii, we can see that the parabola of the charge radii in fig. 1 on the proton-rich side comes mainly from the proton distribution. The proton skin appears in proton-rich isotopes. The neutron (proton) skin thickness $(r_n - r_p)$ is illustrated in fig. 3, which shows that there are thick proton skins on the proton-rich side. On the proton-rich side, the proton r.m.s. radii increase rapidly and the curve has a large slope due to the Coulomb repulsion. In figs. 2, 3, we also find the kinks at the neutron magic number $N = 28$ and 50. As isotopes walk across the kink at $N = 50$ to the neutron-rich side, the neutron distribution undergoes a strong increase of spatial extension, which may give rise to possible halos in highly neutron-rich nuclei. We also observe a strong rise of spatial proton extension as the neutron number falls down from $N = 28$.

Since the harmonic-oscillation wave functions at large distances vanish in a Gaussian way, we briefly discuss the results of the Zn isotopes near drip lines that have an exponentially vanishing tail. It is known that a better way to investigate the properties of nuclei near drip lines is the Hartree-Fock-Bogoliubov method in coordinate space [37]. For the present RMF framework, both a deformed relativistic Hartree-Fock-Bogoliubov code in coordinate space and a deformed relativistic Hartree-Bogoliubov code in coordinate space have not been worked out for all the groups. Current deformed RMF calculations are carried out in harmonic bases. For the neutron-rich exotic nuclei studied in this work, the $3s$ state is bound and the unbound states near the Fermi surface have large angular momenta. This means that the large centrifugal potentials may limit the asymptotic behavior of the wave function and the radii of neutrons obtained with a large basis are approximately reasonable if the probability of neutron occupation on unbound levels is small. However, after a sudden rise of unbound-particle number occurs at drip lines, we would say that the radii of a few drip line nuclei from the calculation are not accurate. For the proton-rich exotic nuclei, besides the centrifugal barrier, there is a high Coulomb barrier that may provide a more favorable limit to the asymptotic behavior for protons near the Fermi surface. On the other hand, the total energy is not sensitive to the unbound levels and is still reliable for the exotic nuclei close to the drip lines. This large basis has also been checked in other studies such as refs. [19,21,38]. Of course, it is better to use codes such as the deformed relativistic Hartree-Bogoliubov one in coordinate space for drip line nuclei and the code is yet to be done.

3.3 BCS pairing correlations and drip line nuclei

Pairing correlations are important to explain the odd-even difference of nuclei. Usually pairing correlations are small compared to the mean field and taken into account through the perturbative treatment like the BCS theory. We may here explain the odd-even difference observed in charge radii with the BCS pairing correlations.

Note that we have plotted radii of even and odd Zn isotopes separately. Except for the highly proton-rich side,

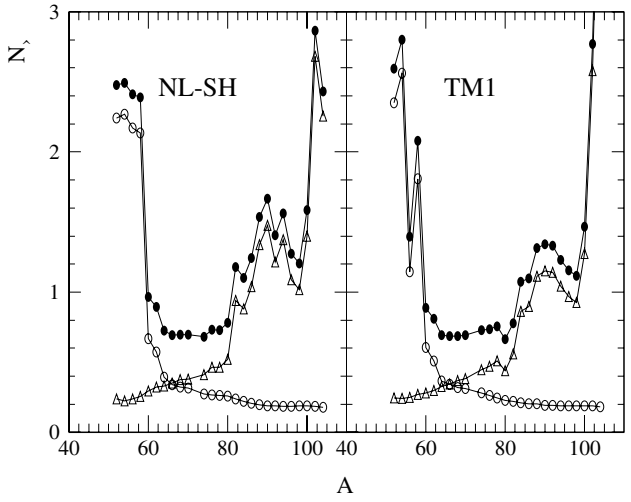

Fig. 4. The occupation number $N_>$ of even Zn isotopes. The open circle stands for the $N_>$ of the proton, the open triangle is for that of the neutron, and the solid circle is for that of the sum of neutron and proton.

the curves for the neutron distribution of odd and even nuclei in figs. 2, 3 almost overlap. The pairing correlation is considered to cause the odd-even difference in charge and matter distributions. The two curves in fig. 1 overlap at the neutron number $N = 50$, where the pairing contribution in even nuclei reduces to the minimum due to the large energy gap at $N = 50$. For highly proton-rich even nuclei, a considerable rate of proton pairs can be boosted to continuum states due to the pairing correlations together with the Coulomb repulsion. We plot the occupation number $N_>$ of positive-energy states in fig. 4. The $N_>$ of the proton goes up sharply from $N = 28$ on the highly proton-rich side. This corresponds to the general trend of the odd-even difference of the charge radii shown in fig. 1. On the neutron-rich side, $N_>$ of the neutron begins to increase from $N = 52$ just after the magic number 50. For highly neutron-rich nuclei, $N_>$ of the neutron undergoes another sharp rise from $N = 70$ which is very close to the neutron drip line. As the neutron number increases, the proton becomes more deeply bound and hence the pairing contribution of the proton reduces, as seen in fig. 4. The odd-even difference of the charge radii decreases as the neutron number rises.

The odd-even difference for the r.m.s. radii should be generally small. Calculations with a spherical RMF code can verify this and show that the odd-even difference for the neutron radii seems larger than that for the proton ones in even-Z isotopes. However, nearly all odd Zn isotopes show large deformations that give rise to the nonzero spatial component of the ω-meson which breaks down the pairs, and that will be discussed in the last subsection and in the appendix. Although the spatial component of the ω-meson is dominated by the unpaired neutron in Zn isotopes, the proton pairs are similarly broken down since the ω-meson is an isoscalar. The Coulomb repulsion pushes out the proton pairs occupying various levels to much more extended distributions in even Zn isotopes on the proton-rich side, and the odd-even difference in the charge radii becomes prominent as nucleon pairs in odd Zn isotopes are broken down. It can still play a pronounced role in pushing out the pairs on the neutron-rich side since the neighboring levels above $Z = 28$ are dense, and that gives rise to a somehow explicit odd-even difference for the charge radii. As mentioned in the beginning of this section, even without considering the vector current, the pairing contribution in odd (deformed) nuclei is very small within drip lines as shown in Pr isotopes [21]. The odd-even difference of the charge radii shown in fig. 1 is reliable for isotopes within drip lines.

It is pointed out in ref. [37] that the BCS treatment will encounter problems associated with nucleon emissions near drip lines where the state density near the Fermi surface is becoming quite dense. The state distribution near the Fermi surface is so dense that the constant pairing gap in the BCS treatment will give rise to the nucleon gas in drip line nuclei. Li *et al.* [21] found that sudden rises of the occupation number $N_>$ occurred beyond drip lines. The perturbative treatment of pairing correlations is no more valid beyond drip lines, since the BCS correction becomes comparable to the mean field. A correct and detailed treatment of pairing correlations is required for drip line nuclei. However, it is beyond the treatment of the present work. It is worthy to notice that the sudden rise of the occupation number $N_>$ is actually a nontrivial signal for the arrival of drip line positions. We can find from fig. 4 that ^{102}Zn is the nucleus where the $N_>$ begins to increase largely. ^{102}Zn may be roughly regarded as the neutron drip line nucleus, which is consistent with the determination from the binding energies. For the proton drip line, it is a little complicated due to the Coulomb repulsion. As similarly judged from fig. 4, the proton drip line would be close to $N = 28$. As shown in fig. 4, the $N_>$ at or beyond the drip lines seems model dependent, and that may be related to the invalidity of the BCS treatment, as discussed above.

The proton and neutron drip line nuclei are determined by the single- and two-nucleon separation energies (s_n and s_{2n}). There is also the odd-even difference of the drip line nuclei. The single-neutron separation energy for odd nuclei becomes negative at $N = 59$, as can be obtained from the values in table 1. ^{87}Zn is the neutron drip line nucleus for odd Zn isotopes. For even isotopes, the drip line is much far off the neutron number $N = 57$. As reported by Li *et al.* [21], the nucleon occupation number at positive states rises dramatically from zero for odd-Z Pr isotopes across the drip lines, which shows that the perturbative treatment of BCS pairing is invalid and a dynamical treatment is required. Though the appropriate consideration of pairing correlations may be important for the drip line nuclei, the position of the neutron drip line for odd isotopes will not change much without considering the pairing correlations. According to the values given in table 1, the even drip line nucleus is ^{102}Zn. For even isotopes with $N > 57$, we can see clearly that there is the relation $s_{2n} < s_n$. This is an implication that even Zn isotopes for $N > 57$ are rich possibly in halos. As shown in fig. 4, the $N_>$ near $A = 88$ reaches a local maximum, which corresponds to a

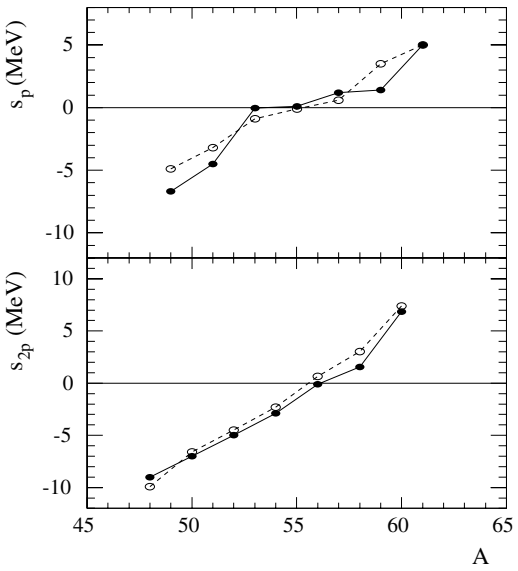

Fig. 5. Single- and two-proton separation energies s_p and s_{2p}. The solid and empty circles are calculated from the NL-SH and TM1 sets, respectively. The determined even and odd drip line nuclei are ^{56}Zn and ^{55}Zn, respectively.

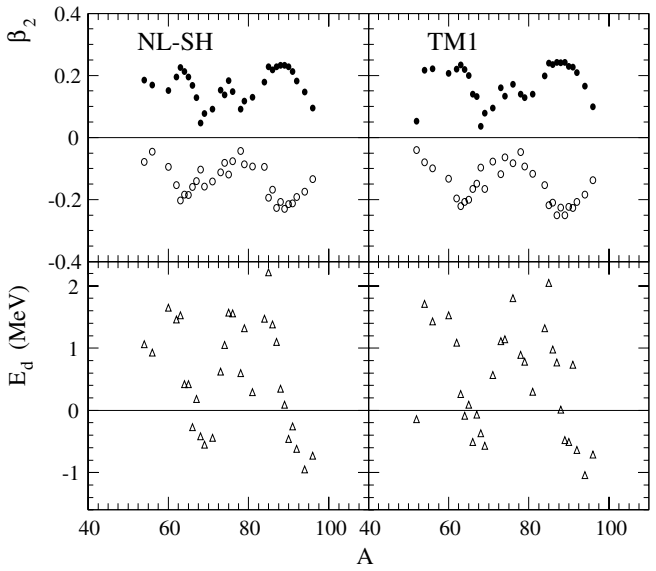

Fig. 6. Shape coexistence of prolate and oblate deformations. The upper panel draws the β_2 of prolate and oblate deformations at each side of the solid line. The lower panel plots the energy difference E_d between the prolate and oblate deformed isotope.

maximum coupling of pairs with the continuum states. It indicates that the appearance of halos may be related to the varying tendency of the odd-even difference.

We go on to obtain the proton drip line of Zn isotopes from the single- and two-proton separation energies (s_p and s_{2p}). Similar to the derivation of the neutron drip line, the s_p for odd nuclei and s_{2p} for even nuclei are calculated. The results are shown in fig. 5. For highly proton-rich even nuclei, the proton occupation number at positive-energy states is so high that the two-proton separation may be much easier. The s_{2p} approaches zero for ^{56}Zn. For odd nuclei, the s_p for ^{55}Zn approaches zero. The experimental proton drip line nucleus is ^{55}Zn [35]. Besides the pairing correlation, the good agreement here may be attributed to the role of the vector current, as will be mentioned later.

3.4 Quadrupole deformations and shape coexistence

Quadrupole deformation parameters (β_2) of Zn isotopes are given in table 2. Except for a few spin-saturated nuclei, all nuclei in this isotopic chain are deformed with the prolate or oblate shape. The spherical isotopes have neutron numbers $N = 28$, 40, 42, 50, 52 and 70, where $N = 28$, 50 are the magic ones, and $N = 70$ is neighboring the position of the neutron drip line. In ref. [17], Lalazissis *et al.* found that the shell closure $N = 28$ for some light isotopic chains, such as Mg, Si, S, Ar, Ti and Cr, is very weak and the shell effects due to $N = 28$ are quenched. However, this does not happen for Zn isotopes. In the Zn isotopic chain, the shell effects associated with the magic numbers are prominent and the shapes at magic numbers are spherical. Both NL-SH and TM1 forces describe well the shell effects and magic closure. Very close agreement of the shape prediction by NL-SH and TM1 forces is shown in table 2.

Usually, quadrupole-deformed nuclei have a prolate or an oblate shape. The Routhian may have many minima which correspond to different deformations, and that allow the shape coexistence of prolate and oblate types but just with a small difference of binding energies for the same nuclei. The Zn isotopic chain is abundant in phenomena of shape coexistence. The dense region for shape coexistence exists for nuclei whose neutrons occupy up to the states just above one magic number but much lower than another magic number. For regions $N = 60$–69 and $N = 84$–96 most of the nuclei have shape coexistence. The energy difference (E_d) of prolate and oblate minima of the shape-coexisting nuclei may be obtained from table 1. In order to show that clearly, we depict the deformations of prolate-oblate shape coexistence together with E_d in fig. 6. There are 65% points in the lower panel falling in the interval $|E_d| < 1\,\mathrm{MeV}$. Usually, the magnitude of E_d for the shape coexistence is about a few hundred keV. In fig. 6, the E_d of ^{85}Zn is $\sim 2.2\,\mathrm{MeV}$. The reason to add this point is that the prolate and oblate minima have the same ground-state configuration.

It is interesting to see that there is a difference of proton and neutron deformations which corresponds to the different deformed mean fields of neutron and proton. The proton and neutron deformations are shown in fig. 7. The difference of proton and neutron deformations goes to the minimum at the neutron magic number $N = 20$, 28 and 50, showing a prominent shell effect. A large difference emerges in the regions near drip lines with $N < 28$ and $N > 50$. Thus, the difference is mainly from the large

Table 2. The quadrupole deformation parameter β_2 of Zn isotopes. The labels I and II are the same as in table 1.

	NL-SH		TM1			NL-SH		TM1	
A	I	II	I	II	A	I	II	I	II
52	0.011	−0.032	0.053	−0.041	75	0.184	−0.119	0.195	
53	0.233		0.247		76	0.148	−0.076	0.172	−0.071
54	0.185	−0.079	0.217	−0.080	77	0.174		0.185	
55	0.244		0.258		78	0.092	−0.043	0.140	−0.047
56	0.169	−0.045	0.222	−0.100	79	0.118	−0.086	0.128	−0.094
57	0.179		0.193		80	0.004		0.006	
58	0.007		0.016		81	0.130	−0.093	0.140	−0.117
59	0.179		0.189		82	0.007	−0.028	0.014	−0.045
60	0.152	−0.095	0.207	−0.133	83	0.193		0.205	
61	0.220		0.231		84	0.179	−0.095	0.199	−0.153
62	0.195	−0.154	0.220	−0.197	85	0.228	−0.194	0.240	−0.219
63	0.226	−0.202	0.234	−0.221	86	0.218	−0.168	0.235	−0.210
64	0.213	−0.184	0.219	−0.207	87	0.228	−0.227	0.242	−0.251
65	0.195	−0.186	0.200	−0.200	88	0.233	−0.207	0.241	−0.226
66	0.168	−0.160	0.140	−0.166	89	0.233	−0.229	0.242	−0.251
67	0.129	−0.140	0.132	−0.149	90	0.228	−0.215	0.229	−0.224
68	0.046	−0.103	0.037	−0.097	91	0.213	−0.212	0.227	−0.227
69	0.077	−0.159	0.078	−0.166	92	0.182	−0.192	0.209	−0.207
70	0.004		0.003		94	0.147	−0.174	0.165	−0.184
71	0.092	−0.141	0.096	−0.077	96	0.096	−0.134	0.099	−0.137
72	0.007		0.005		98	0.011	−0.019	0.011	−0.018
73	0.153	−0.112	0.160	−0.118	100	0.004		0.004	
74	0.137	−0.081	0.134	−0.064	102	0.005		0.006	

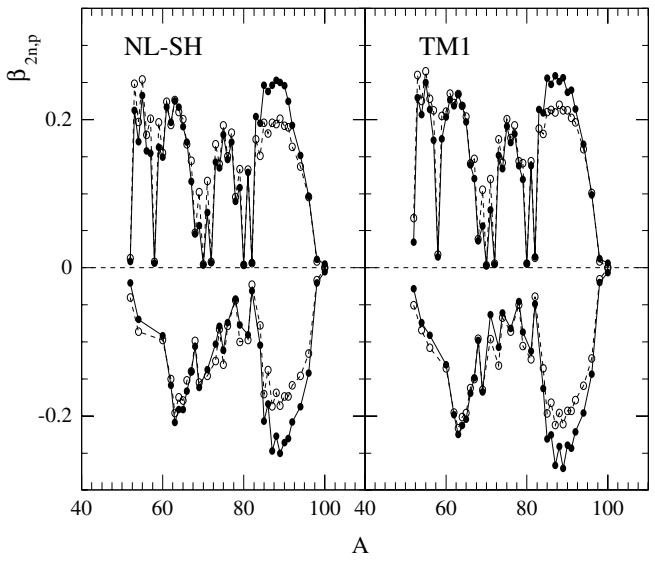

Fig. 7. The neutron and proton quadrupole deformation parameter β_2. The upper part (above the dashed line) is for the prolate deformation and the lower one is for the oblate deformation. The solid and open circles are for neutron and proton deformations, respectively.

excess of nucleons. The proton and neutron deformation difference is large for some odd isotopes, for instance, ^{71,73}Zn, and that may be related to the odd-even difference of nuclear properties.

3.5 Superdeformations in even Zn isotopes

The Nilsson diagram shows that the energy of the orbital $7/2^-[303]$ of $1f_{7/2}$ goes up for the large deformation leading to the orbital intruders at $N(Z) > 26$ [39]. Most Zn isotopes satisfy the relation $N(Z) > 26$. The particle-hole excitations from the $1f_{7/2}$ state below the $N, Z = 28$ shell gap to the orbitals (such as $1g_{9/2}$) above the gap may give rise to deformed secondary minima and collective behaviors. In ref. [28] we investigated the superdeformation in odd Zn isotopes. However, we did not find that there exist ground-state superdeformations in the even Zn isotopes. A possible explanation is that due to pairing correlations the even Zn nuclei are led to more compact shapes due to the nuclear superfluid which is prone to isotropic motions. The SD minima in even Zn isotopes are reasonably expected to appear as the rotational energy term that balances out the potential associated with the large deformation makes the superdeformation possible.

An explicit way to show the occurrence of the superdeformation is to do the constraint calculation as we adjust the pairing gap constant which relates to the strength of pairing correlations. Since the spin of the bandhead of ^{60}Zn is quite low [23], we perform the calculation for ^{60}Zn as an example. In fig. 8, the potential energy surface is given for different pairing gaps in NL-SH. There is an armchaired plateau at $\beta \approx 0.6$ without the reduction of pairing interaction. The SD minimum becomes more stable as the pairing strength is reduced. A self-consistent iteration calculation shows that the SD minimum can be iterated out as long as part (20%) of the pairing correlation contribution is balanced out by the rotational energy. ^{66}Zn is an

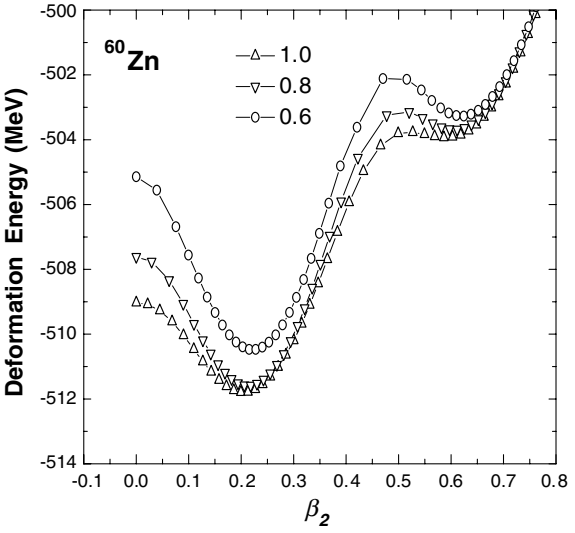

Fig. 8. The Routhian for ^{60}Zn with respect to the quadrupole deformation with the NL-SH set. The coefficient labeled in the figure is the reduction factor of the pairing gap constant. The coefficient 1.0 means no reduction.

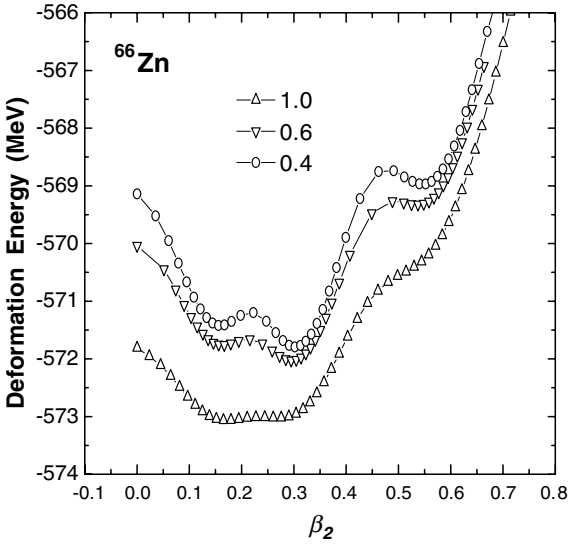

Fig. 9. The same as shown in fig. 8, but for ^{66}Zn.

isotope whose SD band is not observed yet. Figure 9 gives the results of the constraint calculation for a different pairing constant. There is no plateau at the SD region. Compared to ^{60}Zn, it is much more difficult for ^{66}Zn to reach the SD states by the equilibrium established between the rotational energy and the pairing interaction. For other even Zn isotopes, the constraint calculation also indicates that the SD minima may appear as the pairing correlation is partly broken up by the rotational Coliolis force.

The self-consistent calculation shows that the particle occupation number in levels originated from the orbital $1g_{9/2}$ gets a rise and holes appear in $1f_{7/2}$ as the pairing correlation is suppressed by hand in the calculations. The formation of SD minima is mainly attributed to the characteristic configuration of holes in $1f_{7/2}$ and intruder orbitals from $1g_{9/2}$. The calculation with the TM1 set gives similar results.

3.6 The role of the π-meson and vector currents

The π-meson and spatial component of the vector meson have inherent negative parity. For the spin-saturated nuclei, the negative-parity mesons have zero expectation values in the mean-field approximation. In odd nuclei, the time-reversal symmetry is broken and the source term for the negative-parity mesons does not vanish in the mean-field approximation. More particularly, the spatial component of the vector meson has the nonzero value only when the odd or odd-odd nuclei are deformed.

The π-meson, as an isovector scalar meson, plays the contrary role to that of the ρ-meson, say, it shifts down the potential depth of the neutron and shifts up that of the proton. The contribution of the π-meson is small since its source term is dominantly from the valence nucleon. For the Zn isotopes from the proton-rich side to the neutron-rich side the modification to the total binding energy due to the π-meson is about 0.5–0.3 MeV. This small value may be important for giving the value of the neutron separation energies near the drip lines. In lighter nuclei like carbon isotopes, the π-meson contribution to the average quantities, such as deformation parameters, could be comparatively larger [38].

In odd nuclei the spatial component of the ω-meson that couples to the nonzero vector current, brings about the breaking of the time-reversal symmetry. Due to the coupling between the valence neutron and core, the core is polarized and the $\pm\Omega_i$ degeneracy is broken for both neutron and proton orbitals in deformed odd and odd-odd nuclei. The $\pm\Omega_i$ splitting in the Zn isotopic chain is of magnitude 0.1 MeV and it varies with the isospin. For the proton-rich side, the splittings are up to 0.5 MeV between some splitted states. As the neutron number increases, the splitting tends to fall down. Near the neutron drip line the splitting is lower than 0.1 MeV. The source of the spatial ω is mainly from the product of the big and small components of the valence nucleon but with different spin projections (see the appendix). The valence neutron begins to have a definite spin projection due to the weakening residue interactions with core nucleons, and hence the product goes to vanish as the neutron number rises up to the drip line. This explain why the $\pm\Omega_i$ splittings go down with the rise of isospin.

In odd nuclei, the pairing correlation is suppressed due to the blocking effect. Moreover, in deformed odd nuclei, because the $\pm\Omega_i$ degeneracy is broken, the pairs in energy are actually broken up. The vector current in deformed odd nuclei plays the role of anti-pairing. The breaking of $\pm\Omega_i$ degeneracy is eventually prominent for proton-rich isotopes. This can explain the factor that the prediction for the odd nuclei of the proton drip line is in good agreement with the experimental data. However, as the vector current goes to vanish close to the neutron drip line, a consideration of pairing correlations is needed in further investigations.

4 Summaries

We have investigated the ground-state properties of Zn isotopic chain in deformed RMF theory considering the contributions of the π-meson and spatial component of the ω-meson. Binding energies, nuclear sizes, and deformations of whole Zn isotopes have been obtained using the NL-SH and TM1 forces. The two forces predict consistent results for Zn isotopes within drip lines. Theoretical results are in good agreement with the experimental data available.

The shell effects in Zn isotopes are well described in NL-SH and TM1. At the neutron magic number $N = 28$ and 50, kinks in the profile of isotope shifts, relevant to the strong shell effect, have been displayed. An apparent increase of the spatial neutron extension has been observed as the neutron number increases till above the kink at $N = 50$. A similar increase of the spatial proton extension has also been observed as the neutron number falls down from the kink at $N = 28$. The strong shell effect also appears in deformation as the nuclei at neutron magic numbers are sphericized in deformed Zn isotopic chain.

Except for a few spherical nuclei, Zn isotopes have strong deformations. For nuclei of β-stability, the proton and neutron have similar deformation, while the difference of neutron and proton deformations turns out apparent for the regions near drip lines and a few odd nuclei. The difference of proton and neutron deformations is mainly attributed to nucleon excesses. We have found that the Zn isotopic chain is very abundant in shape coexistence of prolate-oblate type. The dense regions having shape coexistence fall on isotopes with a few neutrons off the magic number.

Though the sharp rise of the orbital $7/2^-[303]$ of $1f_{7/2}$ at high deformations may cause the orbital intruders for $N(Z) > 26$, there is no ground-state superdeformation found in even Zn isotopes. The constraint calculation indicates that the SD minimum may appear for some isotopes even at low spins as long as part of the pairing correlation contribution is balanced out by the rotational energy.

Besides keeping even Zn isotopes apart from the superdeformation, pairing correlations are also important for other ground-state properties of even nuclei. The occupation number of positive-energy states rises quickly as the isotope passes drip lines. The neutron drip line nuclei predicted for odd and even nuclei have large difference in neutron number. The drip line reaches $N = 57$ for odd nuclei and $N = 72$ for even nuclei. This obvious odd-even difference may serve as the possible signature of halo formation since the calculation shows that the relation $s_n > s_{2n}$ emerges as $N > 57$ in even nuclei, and that needs an experimental test. The odd-even effect becomes prominent for charge r.m.s. radii on the proton-rich side, as a portion of proton pairs are boosted to the continuum.

The π-meson role in odd Zn isotopes is small. We may expect the π-meson would have larger effects in lighter nuclei. The spatial component of the ω-meson in odd nuclei that couples to the nonzero vector current brings about the breaking of the time-reversal symmetry, leading to splittings of $\pm\Omega$ states. In deformed odd Zn nuclei, because the $\pm\Omega$ degeneracy is broken, the pairs in energy are actually broken down. The vector current in deformed odd nuclei plays the role of anti-pairing. The vector current is important in predicting the proton drip line and odd-even difference of the charge radii.

However, it is a challenge that we use the BCS pairing to perform calculations passing the drip lines. As close to the neutron drip line, the vector current goes to vanish, our work has not treated the pairing interaction for odd nuclei. This deserves further analysis.

This work is partially supported by CAS Knowledge Innovation Project No. KJCX2-N11, the National Natural Sciences Foundation of China under grant Nos. 10405031, 10125521, 10235030 and the Major State Basic Research Development Program under grant No. G200077400.

Appendix A. Source terms of the π-meson and spatial components of vector mesons

We will give the sources of the π-meson together with spatial components of vector mesons in the cylindrical framework. For the axially symmetric nuclei, the following cylindrical frame is used:

$$x = r_\perp \cos\varphi, \quad y = r_\perp \sin\varphi, \quad z = z\,. \tag{A.1}$$

The spinor ψ_i with index i is characterized by the quantum numbers: the total spin projection, parity and isospin Ω_i, π_i, t_i, and it is expanded as follows [10]:

$$\psi(\vec{x})_i = \frac{1}{\sqrt{2\pi}} \begin{pmatrix} f_i^+(z,r_\perp)e^{i(\Omega_i-1/2)\varphi} \\ f_i^-(z,r_\perp)e^{i(\Omega_i+1/2)\varphi} \\ ig_i^+(z,r_\perp)e^{i(\Omega_i-1/2)\varphi} \\ ig_i^-(z,r_\perp)e^{i(\Omega_i+1/2)\varphi} \end{pmatrix}. \tag{A.2}$$

The source terms for the spatial component of ω and ρ mesons are, respectively,

$$\mathbf{j}_{\omega_\varphi} = \sum_{i_1} \frac{1}{2\pi}[f_{i1}^+ g_{i1}^- - f_{i1}^- g_{i1}^+]\,, \tag{A.3}$$

$$\mathbf{j}_{b_\varphi} = \sum_{i_1,t_3} t_3 \frac{1}{2\pi}[f_{i1}^+ g_{i1}^- - f_{i1}^- g_{i1}^+]\,. \tag{A.4}$$

The π-meson source term is explicitly as follows:

$$\rho_\pi = -\left(\nabla_{r_\perp}\rho_{\pi_\perp} + \frac{\rho_{\pi_\perp}}{r_\perp} + \partial_z \rho_{\pi_z}\right), \tag{A.5}$$

where

$$\begin{aligned}\nabla_{r_\perp}\rho_{\pi_\perp} + \frac{\rho_{\pi_\perp}}{r_\perp} = &\sum_i \left(\nabla_{r_\perp} - 2\frac{\Sigma_3 l_3}{r_\perp}\right)(\psi^\dagger(\mathbf{r})\Sigma_{r_\perp}\tau_3\psi(\mathbf{r})) = \\ &\partial_{r_\perp}\sum_{i,t_3}\frac{t_3}{\pi}[f_i^+ f_i^- + g_i^+ g_i^-] \\ &+ \sum_{i,t_3}\frac{t_3}{\pi r_\perp}[f_i^+ f_i^- + g_i^+ g_i^-]\,,\end{aligned} \tag{A.6}$$

$$\partial_z \rho_{\pi_z} = \sum_i \partial_z (\psi^\dagger(\mathbf{r}) \Sigma_3 \tau_3 \psi(\mathbf{r}) = \partial_z \sum_{i,t_3} \frac{t_3}{2\pi} \left[f_i^{2+} - f_i^{2-} + g_i^{2+} - g_i^{2-} \right]. \quad \text{(A.7)}$$

Now we can show on what conditions the π-meson and the spatial component of vector mesons have nonzero contributions. For even nuclei, there exists the time-reversal symmetry. So, if there is the Dirac spinor with positive Ω_i

$$\psi_i \equiv \{ f_i^+,\ f_i^-,\ g_i^+,\ g_i^-;\ \Omega_i \}, \quad \text{(A.8)}$$

it has the time-reversed solution with the same energy

$$T\psi_i \equiv \{ -f_i^-,\ f_i^+,\ g_i^-,\ -g_i^+;\ -\Omega_i \}, \quad \text{(A.9)}$$

where the time-reversal operator is $T = i\sigma_y K$ with σ_y the Pauli matrix and K the complex conjugation operator. We can easily find that the π-meson and the spatial component of vector mesons will vanish for even nuclei where the spin is saturated (*i.e.* states with $\pm\Omega_i$ are filled in pairs) by summing up states with both positive and negative Ω_i's. The nonzero contribution only emerges for odd nuclei where there is one state (Ω_i) whose spin is not paired. In spherical odd nuclei, the structure of the spinor is simplified so that the spinor allows only one independent nonzero component (f^-, g^-) or (f^+, g^+). This makes the source term of the spatial component of vector mesons vanish.

References

1. J.D. Walecka, Ann. Phys. (N.Y.) **83**, 491 (1974).
2. S.A. Chin, J.D. Walecka, Phys. Lett. B **52**, 24 (1974).
3. J. Boguta, A.R. Bodmer, Nucl. Phys. A **292**, 413 (1977).
4. L.N. Savushkin, Sov. J. Nucl. Phys. **30**, 340 (1979).
5. C.J. Horowitz, B.D. Serot, Phys. Lett. B **109**, 341 (1982); Nucl. Phys. A **399**, 529 (1983).
6. B. Banerjee, N.L. Glendenning, M. Guylassy, Nucl. Phys. A **361**, 326 (1981); Ann. Phys. (N.Y.) **149**, 1 (1983).
7. A. Bouyssy, S. Marcos, P.V. Thieu, Nucl. Phys. A **422**, 541 (1984).
8. J.K. Zhang, X.J. Qiu, Phys. Lett. B **152**, 153 (1985); X.J. Qiu *et al.*, Sci. Sin. A **29**, 1283 (1986).
9. P.G. Rheinhard, M. Rufa, J. Maruhn, W. Freiner, J. Friedrich, Z. Phys. A **323**, 13 (1986).
10. Y.K. Gambhir, P. Ring, A. Thimet, Ann. Phys. (N.Y.) **198**, 132 (1990).
11. B.D. Serot, Rep. Prog. Phys. **55**, 1855 (1992).
12. M.M. Sharma, M.A. Nagarajan, P. Ring, Phys. Lett. B **312**, 377 (1993).
13. Y. Sugahara, H. Toki, Nucl. Phys. A **579**, 557 (1994).
14. B.D. Serot, J.D. Walecka, Int. J. Mod. Phys. E **6**, 515 (1997).
15. M.M. Sharma, G.A. Lalazissis, P. Ring, Phys. Lett. B **317**, 9 (1993).
16. G.A. Lalazissis, M.M. Sharma Nucl. Phys. A **586**, 201 (1995).
17. G.A. Lalazissis, A.R. Farhan, M.M. Sharma, Nucl. Phys. A **628**, 221 (1998).
18. G.A. Lalazissis, M.M. Sharma, P. Ring, Nucl. Phys. A **597**, 35 (1996).
19. Z.Z. Ren, Z.Y. Zhu, Y.H. Cai, G.O. Xu, Nucl. Phys. A **605**, 75 (1996).
20. M.M. Sharma, S. Mythili, A.R. Farhan, Phys. Rev. C **59**, 1379 (1999).
21. J.Q. Li, Z.Y. Ma, B.Q. Chen, Y. Zhou, Phys. Rev. C **65**, 064305 (2002).
22. C.E. Svensson, C. Baktash, J.A. Cameronet *et al.*, Phys. Rev. Lett. **79**, 1233 (1997).
23. C.E. Svensson, D. Rudolph, C. Baktash *et al.*, Phys. Rev. Lett. **82**, 3400 (1999).
24. M. Devlin, A.V. Afanasjev, R.M. Clark *et al.*, Phys. Rev. Lett. **82**, 5217 (1999).
25. C.H. Yu, C. Baktash, J. Dobaczewski *et al.*, Phys. Rev. C **62**, 041301(R) (2000).
26. Y. Sun, J.Y. Zhang, M. Guidry, C.L. Wu, Phys. Rev. Lett. **83**, 686 (1999).
27. C.H. Yu, C. Baktash, J. Dobaczewski *et al.*, Phys. Rev. C **60**, 031305 (1999).
28. W.Z. Jiang, T.T. Wang, Z.Y. Zhu, Phys. Rev. C **68**, 047301 (2003).
29. C.E. Price, G.E. Walker, Phys. Rev. C **36**, 354 (1987); R.J. Furnstahl, C.E. Price, G.E. Walker, Phys. Rev. C **36**, 2590 (1987).
30. J.K. Zhang, D.S. Onley, Phys. Lett. B **212**, 145 (1988).
31. J.K. Zhang, D.S. Onley, Nucl. Phys. A **526**, 245 (1991).
32. R.J. Furnstahl, C.E. Price, Phys. Rev. C **41**, 1792 (1990).
33. L.S. Warrier, Y.K. Gambhir, Phys. Rev. C **49**, 871 (1994).
34. P. Möller, J.R. Nix, Nucl. Phys. A **536**, 20 (1992).
35. G. Audi, A.H. Wapstra, Nucl. Phys. A **565**, 1 (1993).
36. M.M. Sharma, G.A. Lalazissis, J.König, P. Ring, Phys. Rev. Lett. **74**, 3744 (1995).
37. J. Dobaczewski, W. Nazarewicz, T.R. Werner *et al.*, Phys. Rev. C **53**, 2809 (1996).
38. W.Z. Jiang, Z.Z. Ren, Z.Y. Zhu *et al.*, Commun. Theor. Phys. (Beijing) **41**, 79 (2004).
39. T. Bengtsson, I. Ragnarsson, Nucl. Phys. A **436**, 14 (1985).